Environmental Science
Processes & Impacts

Temperature dependence of the gas-particle partitioning of selected VOCs

Journal:	*Environmental Science: Processes & Impacts*
Manuscript ID	EM-ART-05-2021-000176.R2
Article Type:	Paper

Temperature dependence of the gas-particle partitioning of selected VOCs

Jeonghyeon Ahn, Guiying Rao, and Eric Vejerano

Center for Environmental Nanoscience and Risk, Department of Environmental Health Sciences, University of South Carolina, Columbia, 29208

Keywords: *enthalpy; entropy; atmospheric aerosols; succinic acid; ammonium sulfate; organic; inorganic*

Environmental Significance

Emissions and accumulation of volatile organic compounds (VOCs) in the atmosphere continue to increase despite successes in limiting their emission from mobile sources. Although the majority of the mass fraction of VOCs remain in the gas phase, a substantial amount can partition into atmospheric particles at levels comparable to those of less volatile contaminants. VOCs that partition in atmospheric particles can be deposited to regions of the respiratory system that are typically inaccessible to that in the gas phase. However, the gas-particle partitioning process is affected by atmospheric temperature. This study will inform the accurate assessment of VOCs' partitioning behavior and hence their environmental and human health relevance.

Temperature dependence of the gas-particle partitioning of selected VOCs

*Jeonghyeon Ahn, Guiying Rao, and Eric Vejerano**

Center for Environmental Nanoscience and Risk, Department of Environmental Health Sciences, University of South Carolina, Columbia, 29208

***Corresponding Author.** *921 Assembly St., PHRC 501D, Columbia, SC, 29208, Tel: +1 (803) 777 6360; e-mail: vejerano@mailbox.sc.edu.

ORCID

Jeonghyeon Ahn

0000-0003-1154-1876

Guiying Rao

0000-0002-6108-9438

Eric Vejerano

0000-0002-6737-9057

Temperature dependence of the gas-particle partitioning of selected VOCs

*Jeonghyeon Ahn, Guiying Rao, and Eric Vejerano**

Center for Environmental Nanoscience and Risk, Department of Environmental Health Sciences, University of South Carolina, Columbia, 29208

Keywords: *enthalpy; atmospheric aerosols; succinic acid; ammonium sulfate; organic; inorganic*

Abstract

The gas-particle partitioning coefficients for volatile organic compounds (VOCs) are difficult to acquire because discriminating the small mass fraction of the VOCs in the aerosol particle relative to that in the gas phase is challenging. In this paper, we report the temperature dependence of the gas-particle partitioning coefficient (K_p) for *n*-butanol (*n*-BuOH) and trichloroethylene (TCE). Using the bench-scale system that we developed, we measured the K_p of surrogate VOCs, *n*-BuOH, and TCE onto inorganic (ammonium sulfate, Am Sulf) and organic (succinic acid, SA) aerosol particles at a fixed relative humidity (RH) of 35%. At this RH level and temperature range of 278.15-308.15 K, the *ln* K_p for TCE and *n*-BuOH partitioning on SA aerosol particles were -27.0 ± 0.70 to -27.9 ± 0.01 and -13.9 ± 0.03 to -17.4 ± 0.17. In contrast, the *ln* K_p for TCE and *n*-BuOH partitioning on Am Sulf aerosol particles ranged from -26.4 ± 0.70 to -27.4 ± 0.71 and -14.1 ± 0.03 to -17.1 ± 0.17, respectively. Results showed that TCE fitted well with the classic van't Hoff relationship. The enthalpy of desorption (ΔH_{des}) for TCE was constant over the temperature range of 278.15 K to 308.15 K, behaving similarly to 1,2-dichlorobenzene. At a similar temperature range, *n*-BuOH partitioning into both aerosol particles exhibited nonlinear temperature dependence. The minimum ratio of ΔH_{des} (Am Sulf:SA) for *n*-BuOH partitioning on each aerosol type was at ~278.15 K. The magnitude of the entropy ΔS_{des} for all VOCs was <1 kJ mol^{-1}.

1. Introduction

As a class of compounds with high vapor pressure and low boiling point (<513 K at standard atmospheric pressure), only a low mass fraction of volatile organic compounds (VOCs) partition onto aerosol particles.[1] For this reason, few studies have investigated the mechanism and extent of partitioning onto aerosol particles for VOCs.[2] The numerous studies on the partitioning mechanism and the models developed to predict the gas-particle partitioning (K_p) coefficients of organic compounds have focused on semivolatile organic compounds (SVOCs).[3–7] Although the extent of aerosol particle partitioning for VOCs is less than SVOCs, VOCs dominate the class of atmospheric pollutants emitted from biogenic and anthropogenic sources. Biogenic VOCs emitted into the atmosphere exceed those of anthropogenic emission by ~10×.[8] However, a recent study has shown that emissions from volatile chemical products (VCPs) have been increasing; VOC emissions from VCPs are twice as large as those emitted from transportation, with VCPs emitted by the petrochemical industry as one of the largest sources.[9]

Studies have measured that sufficient VOC concentration can exist in ambient particulate matter at a concentration level comparable to very low abundance SVOCs.[10–12] Matsumoto and colleagues detected VOC concentration in ambient aerosol particles sampled from the urban atmosphere, with benzene as the dominant compound.[13] The detection of a substantial fraction of VOCs in aerosol particles has an important impact on human health[14,15] because VOCs in submicron aerosol particles can reach regions of the respiratory system that are typically inaccessible to those in the gas phase. Most gas-phase VOCs are poorly absorbed by cells, therefore, immediately exhaled.[16] Aerosols passed over vapors of acrolein, an extremely volatile compound, induce significant damage and inflammation on lung cells compared to the pure aerosol particles.[16,17] Hence, the impact of the gas-particle partitioning of VOCs should not be ignored.

The gas-to-particle partitioning coefficient, K_p, is a measure of a gaseous compound to partition onto particles,[3] which is described by Equation 1:

$$K_p = \frac{C_p}{C_g \times \mathrm{TSP}}, \quad \mathrm{m^3\ \mu g^{-1}} \qquad (1)$$

where C_p and C_g are the concentration of the organic compound in the particle and gas phases, respectively ($\mu g\ m^{-3}$), and the TSP (total suspended particulate matter) is the mass concentration of the aerosol particles ($\mu g\ m^{-3}$). Discriminating the low mass fraction of VOCs in aerosol particles to the high gas-phase concentration is an experimental challenge. To date, measurement of the gas-particle partitioning of VOCs has been derived from field studies.[13] However, determining K_p *via* field sampling is more likely semiquantitative because it is susceptible to inaccuracies from multiple factors inherent during sampling. For compounds with low K_p, such as VOCs, partitioning between the gas and particle phases is controlled by equilibrium.[18,19] Equilibrium is affected by temperature and modulated by the VOC's nature, such as its solubility and polarity. Within the narrow range of temperature in the lower troposphere, the sorption of compounds with varying polarities on aerosol particles is sensitive to temperature fluctuations.

Although limited to three VOCs,[20] this study provides the partitioning data on these compounds that bracket the wide range of VOC polarity.[20–23] We used *n*-butanol (*n*-BuOH) as a surrogate for moderately polar VOCs and trichloroethylene (TCE) as a surrogate for weakly polar VOCs. We compared the K_p of these compounds with 1,2-dichlorobenzene (1,2-DCB), a representative for nonpolar organics. In our earlier paper,[20] we measured the dependence of K_p with RH. Here, we report our study on the temperature dependence of the K_p at a fixed RH level of 35%. We used two types of aerosols to compare differences in partitioning between organic and inorganic aerosol particles. While aerosol composition varies extensively, here, we measured only the K_p of lab-generated aerosols composed of only water-soluble organic matter (WSOM, *e.g.,* succinic acid) and inorganic aerosols. In this research, the temperature dependence of the gas-particle partitioning coefficients of the two VOCs on two different types of aerosols was measured from 278.15 to 308.15 K at 10 K intervals to derive the enthalpy of desorption. We used a bench-scale system so we can precisely control the temperature and RH.

Results from this study will increase our understanding of the partitioning of VOCs in aerosols. The present data will contribute to VOCs' partitioning data and provide an impetus for other researchers to

conduct similar studies using broader VOC types. Additionally, this set of data can be used to generate models specific to describing VOCs' gas-particle partitioning behavior, which is more likely to differ from SVOCs because of differences in physicochemical properties (i.e., higher vapor pressure, polarity, etc.).

Experimental

Materials

n-BuOH (≥99%) and TCE (≥99%) were purchased from Sigma Aldrich and used without purification. Deuterated analogs of *n*-BuOH (1-butanol-d_{10}, ≥99%) and TCE (trichloroethylene-*d*, ≥99%) were purchased from AccuStandard. Methanol (>99.99%, Fisher Chemical) was used as the solvent for preparing the internal standard (IS) and calibration solutions. Succinic acid (≥99%, Alfa Aesar) and ammonium sulfate (Am Sulf, ≥99%, Sigma) were used to generate organic and inorganic aerosols. Here, Am Sulf and SA refer to the aerosol particles generated from ammonium sulfate and succinic acid, respectively.

Environmental Chamber

The detailed experimental method in this companion paper is described in our previous study.[20] Briefly, we used a cylindrical chamber (volume ~7 L) made of aluminum. The chamber's temperature was maintained by enclosing it in a temperature-controlled cabinet (CEO932, Lunaire Environmental, New Columbia, PA). Fig. 1 illustrates the schematic of the experimental setup. The diluted VOC stream, aerosol, and humid air flows were supplied to the chamber. Dilute *n*-BuOH, or TCE flow streams, were generated by placing a 2-mL amber vial containing 1 mL of the pure VOC liquid in the chamber of a Precision Standard Gas Generator (491M-B, KIN-TEC Laboratories Inc, La Marque, TX). Pure VOC vapor effused through the vial, which was diluted with purified compressed air. Compressed air was purified to remove organics and particles using a hydrocarbon trap and high-efficiency particulate air filter connected to the inlet of the compressed air. The dilute TCE concentration, or *n*-BuOH gas concentration, was 30 ppb in air,

which we used in all the tests in this study. We measured the VOC concentration using the thermal desorption method similar to the procedure described in our previous study.[20] The VOC concentration was monitored every 6 h. We used an identical concentration for 1,2-DCB (30 ppb) in our previous study.[20]

Aerosols were generated by atomizing 200 ppm of succinic acid or 100 ppm ammonium sulfate Sulf dissolved/dispersed in distilled water. The atomizer (TSI 3076, TSI Incorporated, Shoreview, MN) was operated at 2.5 L min^{-1} and 207 kPa using compressed air. All flows were controlled by mass flow controllers (MFCs) that were interfaced with a LabVIEW program. Wet aerosols exiting the atomizer were

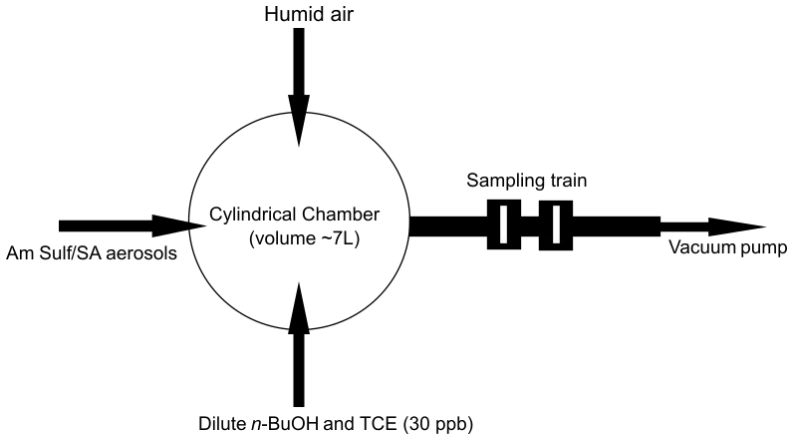

Fig. 1. The schematic of the experimental setup for measuring the gas-particle partitioning of surrogate VOCs.

dried through a diffusion dryer (Model 3062, TSI Inc., Shoreview, MN) containing silica beads as the desiccant.

Humid airflow was generated by mixing the dry air (RH of ~4%) with the wet air. Wet air was generated by bubbling the dry air through two 75-L saturators filled with water that were connected in series. The RH level in the chamber was maintained at 35±3%, which was measured using an RH/temperature probe (USBTENKI-T-RH-CC2, Dracal Technologies, Inc.). According to the companion paper,[20] the decrease in K_p was not significant at higher RHs (>40% RH). Therefore, we fixed the RH level at 35% in this study. The K_p*s* for *n*-BuOH and TCE were obtained at 278.15, 285.15, 298.15, and 308.15

K. The VOC, humid air, and aerosol flow streams were set at 40, 60, and 200 mL min^{-1}, resulting in a total flow rate of 300 mL min^{-1} entering the chamber.

Aerosol characterization

Aerosol properties, including the particle median diameter, particle number concentration, and the total suspended particulate (TSP) were characterized using a scanning mobility particle sizer (SMPS, electrostatic classifier model 3082 with a condensation particle counter model 3775, TSI Incorporated, Shoreview, MN). The dry aerosol mass (TSP) was ~560 μg m^{-3}, which was gravimetrically verified and described elsewhere.[20] The aerosols had a median size of ~77 nm. The SMPS was operated at 300 mL min^{-1} and a sheath flow of 3 L min^{-1}.

Aerosol sampling

Two filter holders connected in series were used for sampling the aerosols/VOCs. Each filter contained a glass microfiber filter (ID ~13 mm, pore size 1.0 μm, Whatman™). The filtration efficiency of one filter was experimentally determined to be ~99.8%.[20] Aerosols were sampled isokinetically at 300 mL min^{-1} using a vacuum pump (Model 6025SE-V, Environmental Monitoring System). The first filter captured the aerosol particles into which the VOC sorbed. The second filter was used to correct the mass fraction of gas-phase VOCs that sorbed onto the filter fibers. We subtracted the VOC mass from the second filter to that from the first filter to calculate the mass that partitioned onto the aerosol particles.

Extraction

After sampling, the two filters were transferred into a separate gas-tight borosilicate vial to extract the VOCs using solid-phase microextraction (SPME). The extraction protocol and quantification were described in detail in our previous study.[20] Briefly, an SPME fiber holder (Supelco™) with a Carboxen®/Poly-dimethylsiloxane (CAR/PDMS) fiber (Supelco™) was inserted into each vial through the Teflon-lined rubber septum of the cap. The SPME fibers were then suspended in the headspace of each vial for 30 min at 295.15 K, and then for another 4 h to ensure a high recovery.

Quantification

The mass of *n*-BuOH and TCE was measured by using a gas chromatograph (Clarus 680, PerkinElmer, Waltham, MA) and mass spectrometer (Clarus SQ8T, PerkinElmer, Waltham, MA) (GC/MS) system for quantification. The calibration curve was generated by preparing different concentrations of *n*-BuOH and TCE solutions in methanol. For each concentration, 1 μL of 1 ppm of the corresponding IS was added. We injected 1 μL of each solution into the GC/MS to measure the peak areas of *n*-BuOH or TCE and the IS. The response ratio *vs.* the mass of *n*-BuOH or TCE was plotted to obtain the calibration curve. The response ratio is the peak area of *n*-BuOH or TCE to that of the IS. For each filter, the VOC masses from the two desorption steps were combined.

The VOCs were identified based on their retention time (2.50±0.1 min for *n*-BuOH, and 2.45±0.1 min for TCE) and their abundant ions (C_2HO^+, $C_4H_8^+$ for *n*-BuOH, and $C_2HCl_3^+$ for TCE) in the mass spectrum. We monitored specific mass-to-charge ratios of 41 and 56 for *n*-BuOH and 130 and 132 for TCE. Mass spectra were acquired in selected ion monitoring mode for trace level detection of the VOCs.

Results and Discussion

Assessing the particle-phase VOCs has been limited by the experimental challenge in detecting the extremely low mass fraction of VOCs in aerosol particles compared to that in the gas phase. Here, we present our study on the quantitative laboratory measurement of K_p of *n*-BuOH and TCE and compare them to our previous results for 1,2-DCB under a fixed RH and varying temperatures.

The *ln* K_p values for the three VOCs are summarized in **Table 1.** The *ln* K_p values for TCE partitioning into SA and Am Sulf aerosol particles at 278.15, 285.15, 298.15, and 308.15 K measured at a fixed RH of 35±3% ranged from -26.4 to -28.3. These values were four to five orders of magnitude lower than the K_p obtained for 1,2-DCB. Whereas the *ln* K_p values for *n*-BuOH ranged from -13.9 to 17.4 on both aerosols. K_p*s* for *n*-BuOH were comparable to that of 1,2-DCB but were ~10× higher at 298.15 and 308.15 K. At 288.15 and 298.15 K, K_p of 1,2-DCB partitioning on Am Sulf aerosol particles was almost two orders of magnitude smaller than those on SA aerosol particles. In general, the *ln* K_p increased as the temperature

increased (K_p decreased with increasing temperature) for all the VOCs partitioning in both aerosol types. In our earlier result for 1,2-DCB, the mass fraction of 1,2-DCB at 308.15 K was below the method's detection limit.

Table 1. Experimental data of *ln* K_p for three VOCs partitioning into aerosols at an RH of 35%

	ln K_p *(SA)*			
VOC	*278.15K*	*288.15 K*	*298.15 K*	*308.15 K*
1,2-DCB[a]	*nm*	-15.9 ± 0.29	-17.0 ± 0.17	-18.5 ± 1.07
TCE	-27.0 ± 0.70	-27.3 ± 0.17	-27.7 ± 1.20	-27.9 ± 0.01
n-BuOH	-13.9 ± 0.03	-14.9 ± 0.09	-15.2 ± 0.02	-17.4 ± 0.17
	ln K_p *(Am Sulf)*			
1,2-DCB[a]	-17.5 ± 0.29	-19.7 ± 0.90	-21.2 ± 0.13	*nm*
TCE	-26.4 ± 0.26	-27.3 ± 0.18	-27.4 ± 0.71	-28.3 ± 0.01
n-BuOH	-14.1 ± 0.16	-14.5 ± 0.17	-15.2 ± 0.17	-17.1 ± 0.12

[a]Data were taken from a companion study for comparison[20]

nm not measured

To deduce the ΔH_{des} and ΔS_{des}, we plotted *ln* K_p with 1/T, which are depicted in **Fig. 2** for the VOC partitioning into Am Sulf aerosol particles, and in **Fig. 3** for those partitioning on SA aerosol particles. On both aerosols types, the sorption of TCE followed the classic van't Hoff relationship (*ln* K_p linearly increased with to 1/T, r^2=0.944) (**Fig. 2 and 3)**.[24] We also observed similar behavior for 1,2-DCB in our earlier report (r^2=0.988). We included the plot for 1,2-DCB for comparison. Partitioning of TCE behaved similarly to 1,2-DCB.[20] However, moderately polar compound *n*-BuOH did not fit well with the classic van't Hoff plot. The r^2 for *n*-BuOH was only ~0.84. We calculated the enthalpy of desorption (ΔH_{des}, kJ mol^{-1}) using Equation 2:

$$\ln K_p = \frac{\Delta H_{des}}{RT} + \frac{\Delta S_{des}}{R} \quad \text{(Equation 2)}$$

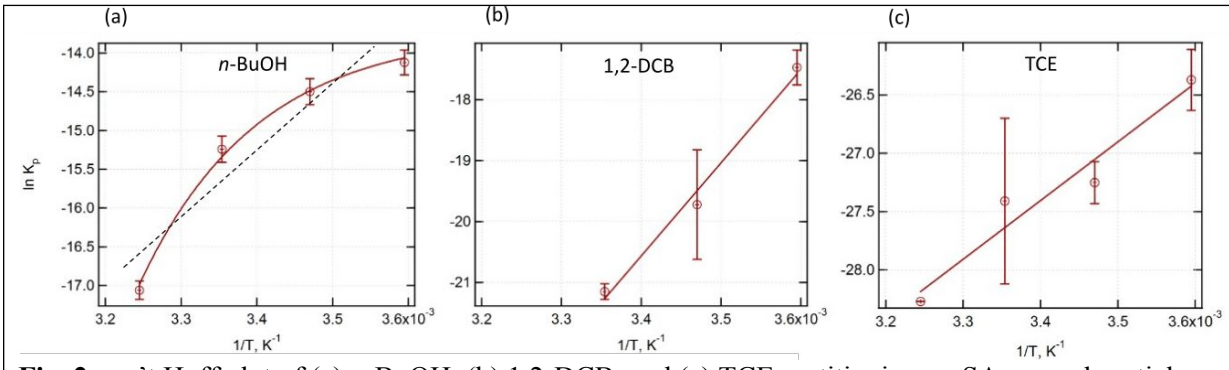

Fig. 2 van't Hoff plot of (a) *n*-BuOH, (b) 1,2-DCB, and (c) TCE partitioning on SA aerosol particles. Data for 1,2-DCB were taken from an earlier study.[20] The red curve is the best-fit function for the data. The black dash line is the linear fit to the data for *n*-BuOH.

where R is the ideal gas constant (J K^{-1} mol^{-1}), and T is the absolute temperature (K). The enthalpy of sorption $(\Delta H_{sorption}) = -\Delta H_{des}$. Values of the linear fitting parameters are summarized in **Table 2**. The slopes of the regression lines for SA and Am Sulf aerosol particles were 11,924 and 15,275, respectively. The enthalpy (ΔH_{des}) and entropy(ΔS_{des}) of desorption were calculated using the following equation, $\Delta H_{des} = R \cdot Slope \cdot 10^{-3}$ and $\Delta S_{des} = R \cdot Intercept \cdot 10^{-3}$, respectively. The estimated ΔH_{des} for TCE on Am Sulf aerosol particles was 34.7 ± 1 kJ mol^{-1}, which was ~4× higher than on SA 7.7± 2 kJ mol^{-1}). Whereas ΔH_{des} values for 1,2-DCB partitioning on Am Sulf aerosol particles were almost similar to that on SA aerosol particles. Fitting the data to a line, 1,2-DCB yielded the highest r^2 (0.993) compared to TCE and *n*-BuOH, in which the latter did not fit well to a line. For all VOCs, $|\Delta S_{des}|$ were < 1 kJ mol^{-1}.

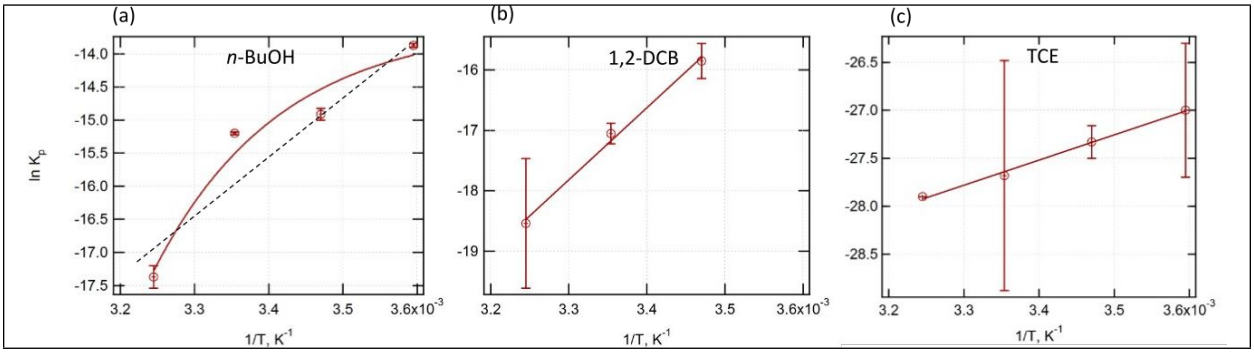

Fig. 3. van't Hoff plot of (a) *n*-BuOH, (b) 1,2-DCB, and (c) TCE partitioning on Am Sulf aerosol particles. Data for 1,2-DCB was taken from an earlier study.[20] The red curve is the best-fit function for the data. The black dash line is the linear fit to the data for *n*-BuOH.

Table 2. Linear fit parameters and thermodynamic values for the three VOCs

	Fitting parameters and thermodynamic value					
VOC	*Intercept*	*Slope* (K)	r^2	ΔH_{des} (kJ mol^{-1})	ΔS_{des} (kJ mol^{-1})	ΔH_{vap*} (kJ mol^{-1})
n-BuOH	-42.9±4 (-46.7±4)	8105±1020 (9183±1080)	0.875 (0.883)	*nc*	*nc*	52.0 ± 3.0[25]
1,2-DCB[a]	-72.8±10 (-61.5±8)	15249±2830 (13173±2420)	0.988 (0.993)	126.8±6 (109.5±5)	-0.60±0.02 (-0.51±0.02)	48.5±0.1[26]
TCE	-41.5±3 (-30.5±3)	4173±958 (924±947)	0.944 (0.995)	34.7±1 (7.7±2)	-0.34±0.01 (-0.25±0.01)	34.7±0.4[27]

Values without and with parentheses are for Am Sulf and SA, respectively. The uncertainty was defined as one standard deviation from the mean. ΔH_{des} and ΔS_{des} were calculated from equation 2 as $\Delta H_{des} = R \cdot Slope \cdot 10^{-3}$ and $\Delta S_{des} = R \cdot Intercept \cdot 10^{-3}$, respectively, where R is the gas constant. *nc* not calculated

*ΔH_{vap} values for the pure VOC in vapor–liquid equilibrium at 298.15 K.

[a]Data were taken from a companion study for comparison.[20]

The factor 10^{-3} appears due to conversion from J to kJ.

Nonlinear temperature dependence observed for *n*-BuOH may be attributed to the interactions with the organic or inorganic aerosol particles or a different three-dimensional structure of *n*-BuOH due to its interaction with the 'bulk' water leading to different enthalpies of interaction.[28] One possible explanation is observed from a computational modeling study on *n*-BuOH/water adsorbing on zeolite composed of silica,[29] which resembles our experimental condition. In our experiment, we fixed RH at 35%, but absolute humidity increases with increasing temperature. DeJaco et al. demonstrate an increasing number of water

molecules form more hydrogen bonds with *n*-BuOH, bridging two *n*-BuOH molecules.[29] Such structures will interact differently with the aerosol resulting in different enthalpies. However, additional investigation is needed to determine if other moderately or strongly polar VOCs behave similarly at this RH level and higher. In this case, the overall dimensionless partitioning coefficient (D_p) can be expressed as

$$D_p = \frac{\sum_{i=1}^{n} C_{p_i}}{C_g} \text{ (Equation 3),}$$

where *i* is the number of distinct *n*-BuOH-water structures in the aerosol particle phase. For simplicity, assuming only two different complexes of *n*-BuOH with water in the aerosol particle phase (C_{p_1} and C_{p_2}) as described above, we define D_p as

$$D_p = \frac{C_{p_1} + C_{p_2}}{C_g} \text{ (Equation 4).}$$

We assume that both complexes have different equilibrium constants,

$$k_1 = \frac{C_{p_1}}{C_g} \text{ (Equation 5)}$$

and

$$k_2 = \frac{C_{p_2}}{C_g} \text{ (Equation 6).}$$

Additionally, we assume that the conformations of *n*-BuOH in the aerosol particle phase are in equilibrium and is defined by

$$k_{2,1} = \frac{C_{p_2}}{C_{p_1}} \text{ (Equation 7).}$$

Dividing the numerator and denominator of Equation 4 by C_{p_1}, and substituting k_1 and $k_{2,1}$ yield,

$$D_p = \frac{1 + k_{2,1}}{k_1^{-1}} \text{ (Equation 8),}$$

which is independent of k_2. Since the equilibrium constants are defined by the Gibbs free energy (ΔG_n^0), which incorporates the dependence of D_p with $1/T$, Equation 8 becomes

$$D_p = \frac{1 + e^{-\Delta G_{2,1}^0/RT}}{e^{\Delta G_1^0/RT}} \text{ (Equation 9),}$$

where R and T are the ideal gas constant and absolute temperature, respectively.

Equation 9 can be expressed as

$$D_p = \frac{1 + e^{-\Delta G_{2,1}^0/RT}}{e^{\Delta G_1^0/RT}} \text{ (Equation 10).}$$

Taking the natural logarithm yields

$$\ln D_p = \ln\left(1 + e^{-\Delta G_{2,1}^0/RT}\right) - \frac{\Delta G_1^0}{RT} \text{ (Equation 11),}$$

which can be expanded as a Taylor series (Supplementary Information) with a general form of

$$\ln D_p = A + Bx + Cx^2 + Dx^4 + Ex^6 \ldots \text{ (Equation 12),}$$

where $x = 1/T$ and $A, B, C, D, E\ldots$ are coefficients.

Since we only have four points, we fitted the data to a second-order approximation. Fitting the data for *n*-BuOH improved the r^2 from 0.875 to 0.980 for Am Sulf and from 0.883 to 0.937 for SA. Values of the fitting parameters a, b, and c are listed in **Table 3**. To determine ΔH_{des} *and* ΔS_{des}, we took the first derivative with respect to x of Equation 12,

$$\frac{\partial \ln D_p}{\partial x} = b + 2cx \text{ (Equation 13).}$$

Since $\frac{\partial \ln K_p}{\partial \frac{1}{T}} = \frac{\Delta H_{des}}{R}$ is the slope in Equation 2, we can approximate that $\frac{\partial \ln D_p}{\partial x} = b + 2cx \cong \frac{\Delta H_{des}}{R}$ therefore,

$$\Delta H_{des} \cong R\left(b + {}^{2c}/_{T}\right) \text{ (Equation 14).}$$

Combining Equations 2, 13, and 14 yield

$$\Delta S_{des} \cong R\left(a - {}^{c}/_{T^2}\right) \text{ (Equation 15).}$$

ΔH_{des} derived from Equation 14 is only a good approximation if $\frac{\partial\, \Delta S_{des\,(T)}}{\partial \frac{1}{T}}$ is close to zero. Equations 14 and 15 have been used to derive thermodynamic values for compounds displaying nonlinear temperature dependence of v'ant Hoff plots.[30]

The ΔH_{des} for *n*-BuOH partitioning on Am Sulf ranged from 16 to 149.9 kJ mol^{-1}. ΔH_{des} exhibited strong temperature dependence, increasing ~10× within a 30 °C/K temperature interval for both aerosol compositions. The gas-particle partitioning on SA had a slightly different ΔH_{des} than on Am Sulf aerosol particles. Similar to the ΔH_{des}, ΔS_{des} exhibited temperature dependence. However, for both aerosol compositions, $|\Delta S_{des}|$ at all temperatures were <1 kJ mol^{-1}. The ΔS_{des} values on both aerosol compositions were all negative, ranging from -0.06 to -0.63 kJ mol^{-1}. Error propagation is described in the Supplementary Information.

Table 3. Fitting parameters for *n*-BuOH using a second-order polynomial

Aerosol	*a*	*b* (×10^5)	*c* (×10^7)	r^2
Am Sulf	-376±45.7	2.03±0.267	-2.85±0.390	0.980
SA	-311±91.9	1.64±0.538	-2.26±0.786	0.937

Experimental data were fitted to equation 11, $\ln K_p = a + bx + cx^2$, where $x = {}^{1}/_{T}$

For the narrow temperature range used in the study, ΔH_{des} for *n*-BuOH partitioning into Am Sulf aerosol particles can be approximated using ΔH_{des} (kJ mol^{-1}) ~4.91T - 1370. The ΔH_{des} for *n*-BuOH ranged from 12.4 to 144.2 kJ mol^{-1} on SA aerosol particles with increasing temperature and followed the equation ΔH_{des} (kJ mol^{-1}) ~ 3.90T - 1062. T is the absolute temperature. The ratio of ΔH_{des} (Am Sulf:SA) partitioning on each type of aerosol increased with increasing temperature, with the ratio being slightly above unity at 300

247 K (**Fig. 4**). Also, ΔH_{des} exhibited a strong temperature dependence from 278 to 300 K. The minimum ratio
248 occurred at the lowest temperature, ~278.15 K.

Table 4. Temperature dependence of ΔH_{des} and ΔS_{des} for *n*-BuOH

T, *K*	$\Delta H_{des,\ Am\ Sulf}$	$\Delta S_{des,\ Am\ Sulf}$	$\Delta H_{des,\ SA}$	$\Delta S_{des,\ SA}$
278.15	16.0±0.6	-0.06±0.01	12.4±3	-0.16±0.03
288.15	43.1±1.7	-0.27±0.01	59.3±14	-0.32±0.06
298.15	98.2±3.7	-0.46±0.02	103.0±24	-0.47±0.09
308.15	149.9±5.7	-0.63±0.02	144.0±34	-0.61±0.12

Using the fitting parameter in Table 4, ΔH_{des} and ΔS_{des} in kJ mol^{-1} were calculated as $\Delta H_{des} \cong R\left(b + {}^{2c}/_{T}\right) \times 10^{-3}$ and $\Delta S_{des} \cong R\left(a - {}^{c}/_{T^2}\right) \times 10^{-3}$, respectively, where R is the gas coefficient. The factor 10^{-3} appears because of the conversion from J to kJ.

249 Partitioning of the VOCs on SA was less endothermic than on Am Sulf aerosol particles as the
250 temperature increased. However, these values were more endothermic than the measured ΔH_{des} for more
251 than 50 S/VOCs partitioning onto atmospheric aerosols. The majority of the ΔH_{des} ranged from 40 to 70 kJ

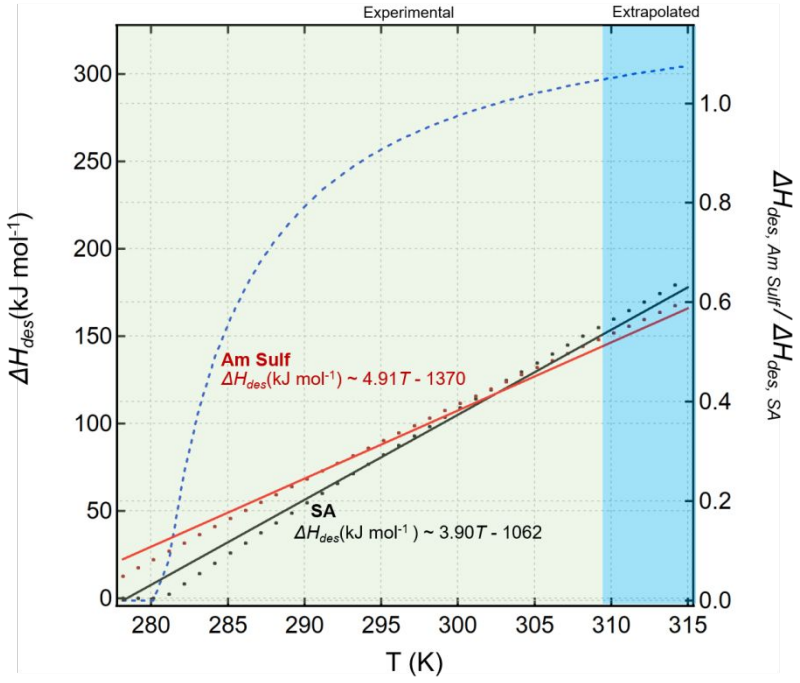

Fig. 4. Temperature dependence of $\Delta H_{des,}$ for the partitioning of *n*-BuOH on Am Sulf (red line) and SA aerosols (black line). The blue curve is the ratio of ΔH_{des} for the VOCs partitioning in Am Sulf and SA aerosols. The green region is the calculated value within the experimental temperature range and values on the blue region are the extrapolated above 308 K.

mol^{-1} [31] for aerosols obtained from diverse environments.[31] Sorption of the VOCs into both types of aerosol were both favorable as deemed from their higher endothermic ΔH_{des} compared to some SVOCs that partitioned into atmospheric aerosols.[31] The calculated values for the amount of VOCs were larger than those reported for a select class of VOCs measured from urban aerosols.[12] VOCs associate with fine particles (d_p<2.5 um).[12,13] Matsumoto and colleagues showed that the aerosol's VOC loading depends strongly on the aerosol mass than the VOCs' gas-phase concentration.[12,13] Measurement of the K_p values for VOCs remained scant. The limited study that measured them was acquired from field sampling that is susceptible to dynamic and static factors (e.g., wind speed, RH, temperature, sampling artifacts, non-equilibrium condition, etc.) confounding the measured gas-particle coefficients' accuracy.[32,33]

On Am Sulf aerosol particles, TCE matched the ΔH_{vap} (34.7±0.4 kJ mol^{-1}) closely with ΔH_{des} (34.7±1 kJ mol^{-1}). The excellent agreement between the ΔH_{des} obtained from our experimental data and the ΔH_{vap} obtained from the National Institute of Standards and Technology (NIST) for TCE on Am Sulf demonstrates that our experimental system was accurate. Arp and colleagues have recommended using the enthalpy of vaporization (ΔH_{vap}) for estimating K_p since the average values of the ΔH_{vap} and ΔH_{des} are close.[31] However, this recommendation cannot be generalized and may only apply to weakly polar compounds. For 1,2-DCB, there is a substantial difference between these parameters. Even more so for *n*-BuOH; ΔH_{des} exhibited a nonlinear temperature dependence on organic and inorganic aerosols as depicted in Figs. 2 and 3. We expect these differences to be larger for complex aerosols relative to the simple model aerosols used in this study.

Although the typical RH range at the lower troposphere is ~70-80%,[34] we determined the temperature dependence at RH ~35%, since, in our earlier study,[20] the VOC's mass fractions above this RH were not significantly different. Additionally, the state of Am Sulf aerosol was most likely a crystalline solid since ammonium sulfate effloresces at ~35–40% RH.[35] However, at RH ~35%, the absolute humidity approximately doubles for each 10 ^{o}C/K rise in temperature. The absolute humidity is ~8× at 308.15 K relative to that at 208.15 K. At this condition, the aerosol can transform into a supersaturated liquid

electrolyte solution depending on the aerosol's inorganic components. Although, for SA and Am Sulf aerosols, such a state is less likely because of their high deliquescence RH. At 298.15 K, small SA (<100 nm) and Am Sulf aerosols deliquesce only at RH of ~99% [36] and ~82%,[37] respectively, because of the Kelvin effect. Therefore, the aerosol's state will most likely be a crystalline solid at RH~70%. Additionally, dry SA particles are less hygroscopic compared to Am Sulf aerosol. For Am Sulf aerosols,[38] water molecules will cover the aerosol's active sites, thus compete with the VOC for adsorption.

Ammonium sulfate and SA aerosol particles more likely exist as crystalline solids at an RH lower than the deliquescence RH. If only a monolayer of water molecules on the surface of particles, there may be competition for active sites, and partitioning is driven by adsorption. Equation 16 depicted the adsorptive part of the saturated vapor pressure (P_i^0) model described by Pankow.[3]

$$K_p = \frac{N_s\, a_{TSP}\, T\, e^{(Q_l - Q_v)RT}}{16\, P_i^o} \text{ (Equation 16),}$$

where P_i^0 is the vapor pressure of compound *i, R* is the gas constant (8.314×10^{-3} kJ mol^{-1} K^{-1}), *T* (K) is the absolute temperature, N_s (mol cm^{-2}) is the surface concentration of sorption sites, a_{TSP} (cm^2 μg^{-1}) is the specific surface area for the TSP; Q_s (kJ mol^{-1}) is the enthalpy for desorption of compound *i* from the adsorbing solid surface (always positive), Q_v (kJ mol^{-1}) is the enthalpy for vaporization of compound *i* as a liquid (always positive). If significant layers of water cover the particle's surface, or if the particles consist of a supersaturated liquid electrolyte solution, particularly at higher RH level, then the partitioning mechanism will be absorptive as described by Equation 17,

$$K_p = \frac{760\, f_i RT}{10^6 MW_i \zeta_i P_i^o} \text{ (Equation 17),}$$

where f_i is the inorganic/organic fraction of the aerosol particle, ζ_i, is the activity coefficient of compound *i* in inorganic/organic matter fraction, MW_i (g mol^{-1}) is the molecular weight of inorganic/organic matter, P_i^0 is the vapor pressure of compound *i*, *R* is the gas constant (8.314 J mol^{-1} K^{-1}), and *T (K)* is the absolute temperature. Although we experimented with only one TSP level, K_p will increase linearly with TSP (a_{TSP}) due to the increasing number of active sites (N_s). Hygroscopic aerosol particles such as ammonium sulfate

are likely to be covered by a thicker water layer. At lower RH and temperature, we attribute the high K_p to the aerosol's higher active surface sites[38] because of less competition with water molecules due to their low concentration. For an aerosol consisting of multiphase systems, the hydrophobic phase may provide a large partitioning matrix for a VOC.

Partitioning is not only affected by the VOC's nature (e.g., solubility and polarity). Aerosol-specific properties, which are dependent on the components contained in them, will also modulate VOC partitioning. The ad/absorptive partitioning will depend on whether the process occurs onto or into solid, or (aqueous) organic or inorganic solution phases, and the composition of those phases or phase transitions as a function of temperature and aerosol composition. In this study, we generated aerosols consisting only of a single solute. Ambient atmospheric aerosols contain multiple components that form multiphase systems depending on environmental conditions, more importantly, RH. Aerosol consisting of an equimolar amount of ammonium sulfate and nitrate drastically deliquesces at a lower RH (63.6%);[39,40] therefore, will affect VOC partitioning differently from a model aerosol consisting of one solute. Phase separations have been known to correlate well with the O:C ratio.[41–43] Aerosols containing ammonium sulfate and less-oxidized organic components (O:C < 0.5) undergo phase separation,[43] whereas aerosols with O:C >0.8 (relatively more oxidized) do not.[43] These types of aerosol are good models to investigate the effect of phase separation on partitioning.

Phase separation can result in aerosols with different morphologies: homogeneous, core-shell, partially engulfed, or structures containing multiple inclusions.[44,45] Depending on the dominant morphology, sorption of VOCs will result in significantly different gas/particle enthalpies due to differences in the VOC's interaction with phase-separated components. Modeling studies should not neglect the contribution of slightly water-soluble organic fraction of aerosols to overall VOC partitioning to prevent underestimating the K_p of VOCs.[20] Since we used a simple aerosol model, the observed K_p and partitioning behavior should be carefully interpreted when applying them to complex aerosols to prevent misattribution

to VOC-specific properties alone. Future studies should incorporate a more complex model aerosol to determine partitioning enthalpies due to combined aerosol- and VOC-specific properties and behaviors.

For a weakly polar organic (TCE), K_p varied linearly with the inverse of the absolute temperature. In contrast, *n*-BuOH, a moderately polar compound, followed a Langmuir-type behavior. Our results differed from those of Matsumoto and colleagues that concluded that the VOCs' gas-particle partitioning did not exhibit temperature dependence.[13] In their study, the K_p*s* were very weakly and negatively correlated with ambient temperature and RH.[13] The reason for their conclusion is that they measured primarily nonpolar and weakly polar VOCs. Therefore, their finding should not be generalized because it appears that the VOC's polarity affects temperature dependence. One reason for this non-sensitivity is the inherent limitation of the field sampling technique; environmental factors such as temperature and RH cannot be controlled compared to their precise modulation in a laboratory setting.

Conclusions

As a dominant class of outdoor and indoor air pollutants, VOCs' environmental and health impacts need to be reexamined. We employed our previously developed method to discriminate the low mass fraction of the VOCs in aerosols to their gas-phase concentration. Using this method enabled us to accurately determine the mass fraction of three surrogate VOCs on simple organic and inorganic aerosols. For a highly abundant VOC, its mass fraction in aerosols can reach a similar level to some SVOCs with very low abundance in the atmosphere, consistent with earlier findings. For a weakly polar organic, K_p varied linearly with the inverse of the absolute temperature. In contrast, for a moderately polar compound, *n*-BuOH, K_p varied quadratically. The sorption of the VOCs into both types of aerosol was favorable compared to some S/VOCs partitioning onto atmospheric aerosols. Using ΔH_{vap} as a proxy for and ΔH_{des} for calculating K_p cannot be generalized because of the wide differences in polarity for VOCs and the nonlinear dependence of ΔH_{des} on temperature. For weakly polar VOCs, ΔH_{vap} can be used as a surrogate for estimating K_p but may not be suitable for moderately and highly polar organics. In developing models, the nature of VOCs has to be considered, particularly for moderately/highly polar VOCs, as well as aerosol-

specific properties. This study will contribute to creating models for VOCs' gas-particle partitioning that can inform in assessing their environmental and health impacts.

AUTHOR INFORMATION

Corresponding Author

*921 Assembly St., PHRC 501D, Columbia, SC, 29208, Tel: 803 777 6360; e-mail: vejerano@mailbox.sc.edu.

Author Contributions

The manuscript was written through the contributions of all authors. All authors have given approval to the final version of the manuscript. JA and GR designed and performed the experiments, drafted, and revised the manuscript. EV designed the experiments, drafted, revised, and edited the manuscripts.

Funding Sources

This work has been funded by the US Army Research Office (GRANT11970168).

Conflicts of interest

The authors declare no conflicts of interest.

ABBREVIATIONS

n-BuOH, *n*-Butanol; 1-2-DCB, 1,2-dichlorobenzene; GC/MS, gas chromatography/mass spectrometry; IS, internal standard; SMPS, scanning mobility particle sizer; SIM, selected ion monitoring; SPME, solid-phase microextraction; TCE, trichloroethylene; VOCs, volatile organic compounds; SVOCs, semivolatile organic compounds

ORCID

Eric Vejerano

0000-0002-6737-9057

Jeonghyeon Ahn

0000-0003-1154-1876

Guiying Rao

0000-0002-6108-9438

Reference

1 US EPA, Technical overview of volatile organic compounds, https://www.epa.gov/indoor-air-quality-iaq/technical-overview-volatile-organic-compounds, (accessed August 1, 2017).

2 G. Rao and E. P. Vejerano, Partitioning of volatile organic compounds to aerosols: a review, *Chemosphere*, 2018, **212**, 282–296.

3 J. F. Pankow, Review and comparative analysis of the theories on partitioning between the gas and aerosol particulate phases in the atmosphere, *Atmos. Environ.*, 1987, **21**, 2275–2283.

4 K.-U. Goss and S. J. Eisenreich, Sorption of volatile organic compounds to particles from a combustion source at different temperatures and relative humidities, *Atmos. Environ.*, 1997, **31**, 2827–2834.

5 J. F. Pankow and T. F. Bidleman, Effects of temperature, TSP and per cent non-exchangeable material in determining the gas-particle partitioning of organic compounds, *Atmospheric Environ. Part Gen. Top.*, 1991, **25**, 2241–2249.

6 J. F. Pankow, Further discussion of the octanol/air partition coefficient K_{oa} as a correlating parameter for gas/particle partitioning coefficients, *Atmos. Environ.*, 1998, **32**, 1493–1497.

7 K.-U. Goss and R. P. Schwarzenbach, Gas/solid and gas/liquid partitioning of organic compounds: Critical evaluation of the interpretation of equilibrium constants, *Environ. Sci. Technol.*, 1998, **32**, 2025–2032.

8 A. H. Goldstein and I. E. Galbally, *Known and unexplored organic constituents in the earth's atmosphere*, ACS Publications, 2007.

9 B. C. McDonald, J. A. de Gouw, J. B. Gilman, S. H. Jathar, A. Akherati, C. D. Cappa, J. L. Jimenez, J. Lee-Taylor, P. L. Hayes, S. A. McKeen, Y. Y. Cui, S.-W. Kim, D. R. Gentner, G. Isaacman-VanWertz, A. H. Goldstein, R. A. Harley, G. J. Frost, J. M. Roberts, T. B. Ryerson and M. Trainer, Volatile chemical products emerging as largest petrochemical source of urban organic emissions, *Science*, 2018, **359**, 760–764.

10 J. F. Hamilton, P. J. Webb, A. C. Lewis, J. R. Hopkins, S. Smith and P. Davy, Partially oxidised organic components in urban aerosol using GCXGC-TOF/MS, *Atmospheric Chem. Phys.*, 2004, **4**, 1279–1290.

11 O. Khanal and D. Shooter, Qualitative analysis of organics in atmospheric particulates by headspace solid phase microextraction-GC/MS, *Atmos. Environ.*, 2004, **38**, 6917–6925.

12 M. Odabasi, O. Ongan and E. Cetin, Quantitative analysis of volatile organic compounds (VOCs) in atmospheric particles, *Atmos. Environ.*, 2005, **39**, 3763–3770.

13 K. Matsumoto, K. Matsumoto, R. Mizuno and M. Igawa, Volatile organic compounds in ambient aerosols, *Atmospheric Res.*, 2010, **97**, 124–128.

14 D. W. Dockery, C. A. Pope, X. Xu, J. D. Spengler, J. H. Ware, M. E. Fay, B. G. Ferris and F. E. Speizer, An association between air pollution and mortality in six U.S. cities, *N. Engl. J. Med.*, 1993, **329**, 1753–1759.

15 C. A. Pope, M. J. Thun, M. M. Namboodiri, D. W. Dockery, J. S. Evans, F. E. Speizer and C. W. Heath, Particulate air pollution as a predictor of mortality in a prospective study of U.S. adults, *Am. J. Respir. Crit. Care Med.*, 1995, **151**, 669–674.
16 S. Ebersviller, K. Lichtveld, K. G. Sexton, J. Zavala, Y.-H. Lin, I. Jaspers and H. E. Jeffries, Gaseous VOCs rapidly modify particulate matter and its biological effects – Part 1: Simple VOCs and model PM, *Atmos Chem Phys*, 2012, **12**, 12277–12292.
17 S. Ebersviller, K. Lichtveld, K. G. Sexton, J. Zavala, Y.-H. Lin, I. Jaspers and H. E. Jeffries, Gaseous VOCs rapidly modify particulate matter and its biological effects – Part 2: Complex urban VOCs and model PM, *Atmos Chem Phys*, 2012, **12**, 12293–12312.
18 A. S. Ansari and S. N. Pandis, The effect of metastable equilibrium states on the partitioning of nitrate between the gas and aerosol phases, *Atmos. Environ.*, 2000, **34**, 157–168.
19 H. Mai, M. Shiraiwa, R. C. Flagan and J. H. Seinfeld, Under What conditions can equilibrium gas–particle partitioning be expected to hold in the atmosphere? *Environ. Sci. Technol.*, 2015, **49**, 11485–11491.
20 J. Ahn, G. Rao and E. Vejerano, Partitioning of 1,2-dichlorobenzene onto organic and inorganic aerosols, *Environ. Chem.*, , DOI:https://doi.org/10.1071/EN21016.
21 T. Salthammer, Very volatile organic compounds: an understudied class of indoor air pollutants, *Indoor Air*, 2016, **26**, 25–38.
22 M. Jang, N. M. Czoschke and A. L. Northcross, Atmospheric organic aerosol production by heterogeneous acid-catalyzed reactions, *ChemPhysChem*, 2004, **5**, 1646–1661.
23 H. P. H. Arp, R. P. Schwarzenbach and K.-U. Goss, Ambient gas/particle partitioning. 1. Sorption mechanisms of apolar, polar, and ionizable organic compounds, *Environ. Sci. Technol.*, 2008, **42**, 5541–5547.
24 K. U. Goss, Adsorption of organic vapors on ice and quartz sand at temperatures below 0 °C, *Environ. Sci. Technol.*, 1993, **27**, 2826–2830.
25 PubChem, 1-Butanol, https://pubchem.ncbi.nlm.nih.gov/compound/263, (accessed May 20, 2021).
26 NIST, Benzene, 1,2-dichloro-, https://webbook.nist.gov/cgi/cbook.cgi?ID=C95501&Mask=6FF, (accessed May 20, 2021).
27 NIST, Trichloroethylene, https://webbook.nist.gov/cgi/cbook.cgi?ID=C79016&Mask=4, (accessed May 20, 2021).
28 M. Tanase, A. Soare, V. David and S. C. Moldoveanu, Sources of nonlinear van't Hoff temperature dependence in high-performance liquid chromatography, *ACS Omega*, 2019, **4**, 19808–19817.
29 R. F. DeJaco, P. Bai, M. Tsapatsis and J. I. Siepmann, Adsorptive separation of 1-butanol from aqueous solutions using MFI- and FER-type zeolite frameworks: A Monte Carlo study, *Langmuir*, 2016, **32**, 2093–2101.
30 T. Galaon and V. David, Deviation from van't Hoff dependence in RP-LC induced by tautomeric interconversion observed for four compounds, *J. Sep. Sci.*, 2011, **34**, 1423–1428.
31 H. P. H. Arp, R. P. Schwarzenbach and K.-U. Goss, Ambient gas/particle partitioning. 2: The influence of particle source and temperature on sorption to dry terrestrial aerosols, *Environ. Sci. Technol.*, 2008, **42**, 5951–5957.
32 K. Kristensen, M. Bilde, P. P. Aalto, T. Petäjä and M. Glasius, Denuder/filter sampling of organic acids and organosulfates at urban and boreal forest sites: Gas/particle distribution and possible sampling artifacts, *Atmos. Environ.*, 2016, **130**, 36–53.
33 Z. Wang, Z. Xie, A. Möller, W. Mi, H. Wolschke and R. Ebinghaus, Atmospheric concentrations and gas/particle partitioning of neutral poly- and perfluoroalkyl substances in northern German coast, *Atmos. Environ.*, 2014, **95**, 207–213.
34 A. Ruzmaikin, H. H. Aumann and E. M. Manning, Relative humidity in the troposphere with AIRS, *J. Atmospheric Sci.*, 2014, **71**, 2516–2533.
35 V. G. Ciobanu, C. Marcolli, U. Krieger, A. Zuend and T. Peter, Efflorescence of ammonium sulfate and coated ammonium sulfate particles: Evidence for surface nucleation, *J. Phys. Chem. A*, 2010, **114**, 9486–9495.

36 M. Bilde and B. Svenningsson, CCN activation of slightly soluble organics: the importance of small amounts of inorganic salt and particle phase, *Tellus B Chem. Phys. Meteorol.*, 2004, **56**, 128–134.
37 S. D. Brooks, M. E. Wise, M. Cushing and M. A. Tolbert, Deliquescence behavior of organic/ammonium sulfate aerosol, *Geophys. Res. Lett.*, 2002, **29**, 23-1-23–4.
38 K.-U. Goss and R. P. Schwarzenbach, Quantification of the effect of humidity on the gas/mineral oxide and gas/salt adsorption of organic compounds, *Environ. Sci. Technol.*, 1999, **33**, 4073–4078.
39 I. N. Tang and H. R. Munkelwitz, Composition and temperature dependence of the deliquescence properties of hygroscopic aerosols, *Atmospheric Environ. Part Gen. Top.*, 1993, **27**, 467–473.
40 L. Wu, X. Li and C.-U. Ro, Hygroscopic behavior of ammonium sulfate, ammonium nitrate, and their mixture particles, *Asian J. Atmospheric Environ.*, 2019, **13**, 196–211.
41 M. A. Dallemagne, X. Y. Huang and N. C. Eddingsaas, Variation in pH of model secondary organic aerosol during liquid–liquid phase separation, *J. Phys. Chem. A*, 2016, **120**, 2868–2876.
42 Y. You, M. L. Smith, M. Song, S. T. Martin and A. K. Bertram, Liquid–liquid phase separation in atmospherically relevant particles consisting of organic species and inorganic salts, *Int. Rev. Phys. Chem.*, 2014, **33**, 43–77.
43 Y. You, L. Renbaum-Wolff, M. Carreras-Sospedra, S. J. Hanna, N. Hiranuma, S. Kamal, M. L. Smith, X. Zhang, R. J. Weber, J. E. Shilling, D. Dabdub, S. T. Martin and A. K. Bertram, Images reveal that atmospheric particles can undergo liquid-liquid phase separations, *Proc. Natl. Acad. Sci.*, 2012, **109**, 13188–13193.
44 N.-O. A. Kwamena, J. Buajarern and J. P. Reid, Equilibrium morphology of mixed organic/inorganic/aqueous aerosol droplets: investigating the effect of relative humidity and surfactants, *J. Phys. Chem. A*, 2010, **114**, 5787–5795.
45 M. A. Freedman, Phase separation in organic aerosol, *Chem. Soc. Rev.*, 2017, **46**, 7694–7705.